



# Oriental dependence of the potential of mean force for a discotic liquid crystal near a substrate

Daniel Salgado-Blanco, Carlos I. Mendoza & Enrique Díaz-Herrera

To cite this article: Daniel Salgado-Blanco, Carlos I. Mendoza & Enrique Díaz-Herrera (2020): Oriental dependence of the potential of mean force for a discotic liquid crystal near a substrate, *Molecular Physics*, DOI: [10.1080/00268976.2020.1748241](https://doi.org/10.1080/00268976.2020.1748241)

To link to this article: <https://doi.org/10.1080/00268976.2020.1748241>



Published online: 07 Apr 2020.



Submit your article to this journal [↗](#)

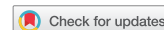


View related articles [↗](#)



View Crossmark data [↗](#)

RESEARCH ARTICLE



# Oriental dependence of the potential of mean force for a discotic liquid crystal near a substrate

Daniel Salgado-Blanco <sup>a</sup>, Carlos I. Mendoza<sup>b</sup> and Enrique Díaz-Herrera<sup>c</sup>

<sup>a</sup>Cátedras CONACyT – Centro Nacional de Supercómputo, Instituto Potosino de Investigación Científica y Tecnológica, San Luis Potosí, México;

<sup>b</sup>Instituto de Investigaciones en Materiales, Universidad Nacional Autónoma de México, Ciudad de México, Mexico; <sup>c</sup>Departamento de Física, Universidad Autónoma Metropolitana-Iztapalapa, Ciudad de México, Mexico

## ABSTRACT

In this work we calculate the potential of mean force for a discotic liquid crystal (DLC) confined in a slab geometry. We have set the reaction coordinate as the distance between a DLC test particle with a fixed orientation and a wall with face-on anchoring. Five different orientations of the DLC test particle are explored, which correspond to parallel and perpendicular orientations with regard to the anchoring promoted by the walls, and three intermediate orientations between the parallel and perpendicular configurations. The potential of mean force reflects the strong effect of the system's anisotropy: particles with the wrong orientation are energetically penalised whilst the particles with the correct orientation are favoured.

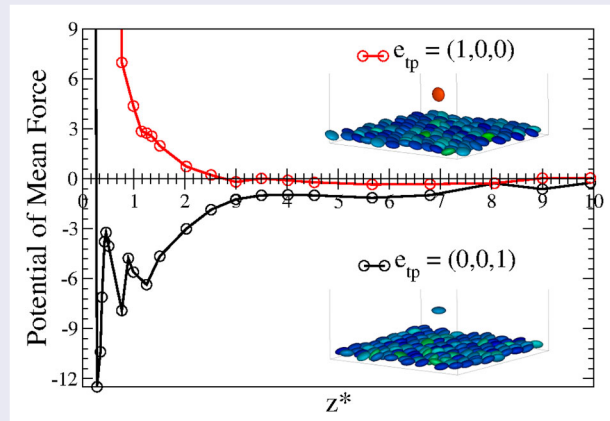
## ARTICLE HISTORY

Received 3 January 2020

Accepted 18 March 2020

## KEYWORDS

Liquid crystals; molecular simulations; potential of mean force



## 1. Introduction

Liquid crystals (LC) are materials which are able to display mesophases, or intermediate phases between the completely disordered isotropic liquid, where all positions and orientations are equivalent, and the more ordered crystalline phase, where the particles form a periodic arrangement. These mesophases are the dominant factor in many of their unique characteristics, such as their electronic, optical and magnetic properties [1–4], or their particular behaviour in flow [5–7]. Among all these properties of liquid crystals, many of them that could be employed in the industry rely on effectively exploiting their characteristic long range orientational order, and

the possibility to change it at will using external fields [8–10].

The transition between different mesophases may not be necessarily connected through an easily accessible phase space trajectory, since, ultimately, the difference between those two stable states are determined by energy barriers, which will have to be overcome in order to pass from one state to the other. These energy barriers are the result of a complicated interplay between the intermolecular forces and the external fields involved. This is also true for fluids under confinement, where the walls operate as an external field which promotes the stratification of the fluid near the walls, independently of the

**CONTACT** Daniel Salgado-Blanco  daniel.salgado@ipicyt.edu.mx  Cátedras CONACyT – Centro Nacional de Supercómputo, Instituto Potosino de Investigación Científica y Tecnológica, Camino a la Presa San José 2055, 78216 San Luis Potosí, México

existence of attraction between the walls and the fluid particles. In the case of liquid crystals, the interaction between the fluid and the walls could promote preferential mesophases, by promoting a particular orientation of the mesogens attached to the walls, a phenomena called anchoring. Such orientation is transferred to the rest of the fluid by intermolecular forces and produce an inhomogenous region whose orientation is fixed by the anchoring of the wall. As we move away from this region the influence of the wall decreases and the system's bulk is recovered.

A walls' anchoring can be obtained by various means, such as photoalignment techniques [11], surface chemistry [12] and topographic patterning [13], only to name a few. Three broad classes of anchorings can be used to describe the type of alignment produced: planar, homeotropic and tilted. In the planar case the director is parallel to the surface, while in the homeotropic anchoring the director lies normal to the surface, finally, in the tilted case, the director is tilted with respect to the surface. When the liquid crystal is constituted by disc-shaped molecules or oblates, such as a liquid crystal composed of triphenylene-core molecules, the homeotropic anchoring results in the discs lying face-on on the surface, while the planar anchoring results in the discs lying edge-on on the surface. The face-on anchoring case, coupled with the ability of the discotic liquid crystals (DLC) to arrange themselves into columnar phases with a promising charge carrier mobility along the column, make the face-on anchoring an interesting configuration, since the column's growth should be normal to the walls and nano-wires connecting both walls are expected.

One theoretical tool that has been extensively used to determine the effect of an inhomogeneous fluid structure on the free energy landscape, is the potential of mean force (PMF) [14–17]. The PMF allows to quantify the change of free energy along one or more reaction coordinates of interest, such as the distance between two particles or the relative orientation between them, only to name a few. Molecular simulations provide several means to calculate the PMF [18–20] for systems that are beyond a purely theoretical description due to its complexity. In the case of LC's the relevance of its orientational order in their use as detectors has resulted in the common practice of calculation of the PMF between colloids and or wall immersed in a LC host. To the best of our knowledge, this methodology has not been previously used to characterise the changes in free energy of the LC itself, although it has been used in the case of an isotropic fluid in order to quantify the change of free energy of a fluid's molecule adsorbed [15].

In this work we present a detailed description of the potential of mean force arising in a system of discotic

liquid crystals confined by two parallel walls (slab geometry) which promote a face-on anchoring. We calculate the potential of mean force for a test particle with different fixed orientations, as function to the distance to the wall.

The paper is structured as follows: Section 2 presents the model used to mathematically describe our system while Section 3 contains the details of the molecular simulation employed. In Section 4 we present the results and the discussion. Finally, the concluding remarks are included in Section 5.

## 2. Model description and working equations

### 2.1. Disc-disc and disc-wall interaction

The system consists of a discotic liquid crystal confined in a rectangular slab of constant volume, where the distance between the walls is denoted by  $L_z$ . The particle-particle [21] and wall-particle [22] interactions are defined by a Gay-Berne pair potential, whose equations and parameters have been fully specified in a previous work [23]. Nevertheless, here we include some basic equations for the benefit of the reader. The particle-particle interaction is defined as:

$$U(\hat{\mathbf{u}}_i, \hat{\mathbf{u}}_j, \hat{\mathbf{r}}_{ij}) = 4\epsilon(\hat{\mathbf{u}}_i, \hat{\mathbf{u}}_j, \hat{\mathbf{r}}_{ij})(\Xi_{ij}^{-12} - \Xi_{ij}^{-6}), \quad (1)$$

where  $\hat{\mathbf{r}}_{ij} = \mathbf{r}_{ij}/r_{ij}$  is the unit vector connecting the centres of particles  $i$  and  $j$ ,  $\hat{\mathbf{u}}_{i,j}$  is the unit vector along the principal axes of discs  $i, j$ , and  $\epsilon$  is a strength anisotropy function. Finally,  $\Xi$  is an anisotropy function which determines the distance between two mesogens.

Following previous works [23] and using the notation proposed by Bates and Luckhurst [24], in this study we have used the parametrisation GB(0.345, 0.2, 1.0, 2.0). This set of parameters promotes the formation of columns of discs, since the strongest attraction between mesogens happens when they approach with their axis parallel to each other and to the vector that connects their centres.

The potential used for the wall-disc interaction has the form:

$$V(z, \theta) = \epsilon_w \left[ \frac{2}{15} \left( \frac{\sigma_{\text{ff}}}{z - z_{\text{shift}}(\theta)} \right)^9 - \left( \frac{\sigma_{\text{ff}}}{z - z_{\text{shift}}(\theta)} \right)^3 \right] \times [1 + AP_2(\cos(\theta))], \quad (2)$$

where  $P_2(x) = \frac{1}{2}(3x^2 - 1)$  is the second-order Legendre polynomial,  $z_{\text{shift}}$  is a function which determines the wall-disc contact distance, and  $\epsilon_w$  is parameter which determines the strength of the anchoring. Finally, the

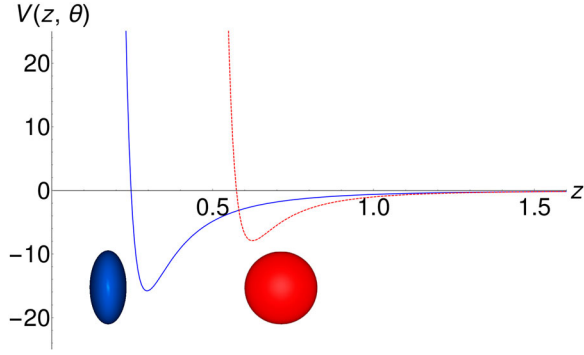


**Figure 1.** Wall-disc interaction potential as given by Equation (2) with the parameters set in this study. The red line corresponds to a particle in a edge-on configuration ( $\theta = \pi/2$ ) approaching to a wall promoting a face-on anchoring ( $A = 1.0$ ), while the blue line corresponds to a particle in a face-on configuration ( $\theta = 0$ ) approaching to a wall promoting a face-on anchoring ( $A = -0.5$ ).

parameter  $A$  determines the type of anchoring. For example,  $A = -0.5$  promotes a planar or edge-on anchoring, while  $A = 1$  encourages an homeotropic or face-on anchoring, as depicted in Figure 1 where we plot  $V(z, \theta)$  as a function of  $z$ , the distance of the particle to the wall. In this work, we set  $A = 1$  (face-on anchoring) and  $\epsilon_w = 10$  for all cases. This value of  $\epsilon_w$  corresponds to a configuration within typical experimental setups (the interested reader may consult Ref. [23], which contains a section with the specific values obtained when translating the reduced unit parameters).

## 2.2. Potential of mean force

The free energy difference  $\Delta W$  between two thermodynamic states can be obtained by [25]

$$W(\lambda_2) - W(\lambda_1) = \int_{\lambda_1}^{\lambda_2} d\lambda' \left\langle \frac{\partial \mathcal{H}}{\partial \lambda'} \right\rangle, \quad (3)$$

where the brackets denote the statistical average over the equilibrium ensemble corresponding to the parameter value  $\lambda'$  and  $\mathcal{H} = \mathcal{H}(\mathbf{r}, \mathbf{p}; \lambda)$  is the Hamiltonian of the system; minus the integral, this quantity is equal to the potential of the mean force, so the potential of the mean force (PMF) provides a measure of the effective difference in free energy between two thermodynamic states, as a function of one or several degrees of freedom [14]. In our case, we calculate the potential of the mean force as the work done on a test particle on going from the centre of the box to a given distance  $z_f$ , varying only the  $z$ -coordinate of the particle. In other words, we set the distance  $z$  as the reaction coordinate.

## 3. Simulation details

Molecular Dynamics simulations have been carried out on an NVT ensemble for 5000 particles inside of a rectangular box. The simulation box presents periodic boundary conditions along the  $x$  and  $y$  directions and is limited along the  $z$  axis by two walls which promote a homeotropic, or face-on anchoring. In this simulations the Nosé–Hoover thermostat [26] was used to held fixed the temperature of the system. The thermostat constant was set at  $Q_t = 10$ .

We have used  $\sigma_0$  and  $\epsilon_0$  as length and energy units, respectively, and standard reduced units ( $T^* = k_B T / \epsilon_0$ ,  $P^* = P \sigma_0^3 / \epsilon_0$  and  $\rho^* = \rho \sigma_0^3$ , where  $k_B$  stands for the Boltzmann constant) for the rest of the system parameters. Equations of translational and orientational dynamics were integrated using the velocity-Verlet algorithm [26] with a reduced time step of  $\delta t = \delta t (\sigma_0^2 m / \epsilon_0)^{-1/2} = 0.0015$  (where  $m = 1$ ).

Simulations on an ensemble  $NP_{xy}T$  system were run at  $T^* = 3$ , and for  $P_{xx}^* = P_{yy}^* = 25$ . These parameters correspond to conditions where the confined fluid presents an isotropic bulk phase [23] and, hence, were used in order to obtain initial equilibrium configurations. In this case, the thermostat constant was set at  $Q_t = 10$ , while the barostat constant used was  $Q_p = 1000$ . The system was simulated for  $1 \times 10^7$  timesteps. The equilibrium density with the corresponding  $x$ – $y$  area of the cell obtained from the  $NP_{xy}T$  ensemble run, was used as the initial state for the  $NVT$  simulations.

The parameters used in this work can be compared with experimental data by the use of reasonable estimates. For example, assuming room temperature, then  $\epsilon_0 \simeq 1.37 \times 10^{-21}$ . Such energy value allows us to estimate the anchoring energy, since the adsorption energy per particle, defined by the minimum of the wall-disc potential. According to Figure 1, for the face-on case,  $E_A \simeq 15\epsilon_0$ . In order to transform the surface energy density, the area of a nematogen in contact with a wall is approximately  $A = \pi \sigma_0^2 / 4$  and considering a value of  $\sigma_0 = 40$  Angstroms which corresponds to the diameter of a triphenylene-based molecule [27], results on a surface energy density of  $3.6 \times 10^{-3}$  Joules/m<sup>2</sup>, which is close to the highest experimental measured anchoring energy, where the experimental values range from  $10^{-6}$  J/m<sup>2</sup> to  $10^{-3}$  J/m<sup>2</sup> [28, 29]. Another useful estimate is the size of the cells, which corresponds to  $L_z = 25\sigma_0 = 100$  nm. This value is also near to the experimental values for confined liquid crystals, which range from confinement lengths of 10–200 nm [30, 31].

In order to calculate the potential of mean force, several runs were made where a DLC test particle (tp) is maintained with a fixed position  $\vec{r}_{tp}$  and orientation  $\hat{e}_{tp}$

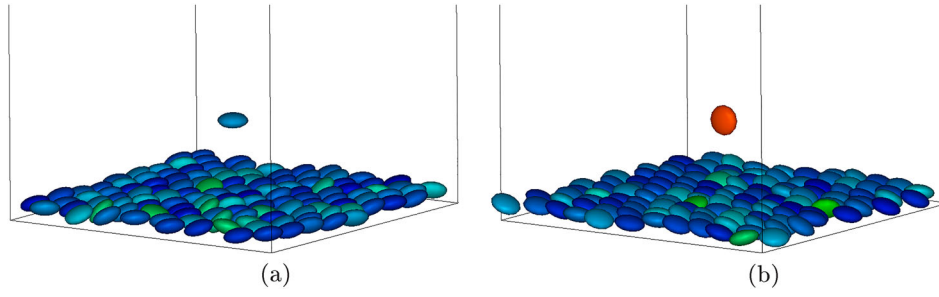


**Figure 2.** A schematic view of a test particle near a wall promoting a homeotropic anchoring. In (a) the mesogen's orientation corresponds to the orientation promoted by the walls, and in (b) the mesogen's orientation is perpendicular to the orientation promoted by the walls. For the sake of clarity, only the test particle and the first layer adjacent to the wall are shown.

(see Figure 2, where a schematic view of two test mesogens near a wall is shown), while interacting with the rest of the system. This is, the orientational and positional dynamics for the rest of the mesogens still consider the test particle. The test particle is used to measure the force felt in the  $z$  direction ( $F_z$ ) by the mesogen due to the rest of the system. At a particular distance away from the wall  $z_{tp}$ ,  $\langle F_z(z_{tp}) \rangle$  is obtained from runs of at least  $1 \times 10^6$  timesteps. Different simulation runs for different distances  $z_{tp}$ , allowed us to obtain the change of free energy by numerical integration. We used two different orientations for a given position: one with the axis of the particle parallel to a wall (equivalent to the order induced by the edge-on anchoring) and one with the axis perpendicular to the wall (equivalent to the order induced by the face-on anchoring). An additional ensemble average was calculated by randomly positioning 25 test particles at the same distance  $z_{tp}$  from the wall, and with the same fixed orientation. Each of the 25 test-particle runs corresponded to an independent simulation box.

The positions  $z_{tp}$  that determined the complete trajectory to be integrated, started near the centre of the box ( $z^* \approx 11$ ) and ended at a short distance from the wall. The minimum wall-mesogen distance where  $\langle F_z(z_{tp}) \rangle$  was measured depends on the orientation of the test particle (the centre of mass of a face-on particle can approach closer to the wall than the centre of mass of the edge-on particle).

#### 4. Results and discussion

In the following, results from simulations are presented: first, showing the results of characterising the structure of the fluid at equilibrium and then the results for the potential of mean force. We have analysed three main scenarios: (a) when the orientation of the test particle is parallel to the orientation promoted by the walls, (b) when it is perpendicular to the orientation promoted by the walls, and (c) three different intermediate orientations between

case (a) and case (b). In all cases we have set the distance from the wall as the reaction coordinate.

Confining a fluid results in a stratification of such fluid near the wall. In this case, two useful quantities for the structural characterisation of the system are the density and order parameter profiles. Given the symmetry of the system we calculated this quantities in the  $z^*$  direction. For the density, we have used the expression  $\rho^*(z) = N_z / (A_{xy} dz)$ , where  $N_z$  is the number of particles in a slab parallel to the wall,  $A_{xy}$  is the area of the box in the  $x$ - $y$  plane and  $dz$  is the width of the bin, which in this case was fixed at  $0.05\sigma_0$ . For the orientational order parameter  $S$ , we calculated  $S$  via the largest eigenvalue of the orientational tensor [32]:

$$\mathbf{Q} = \frac{1}{2N} \sum_{i=1}^N (3\hat{\mathbf{u}}_i \otimes \hat{\mathbf{u}}_i - \mathbf{I}), \quad (4)$$

where  $\otimes$  denotes the tensor product,  $\mathbf{I}$  corresponds to the identity matrix, and  $N$  is the total number of particles contained in the system. The normalised eigenvector corresponding to  $\lambda_{\max}$  is the system director  $\mathbf{n}$ , and  $S = \lambda_{\max}$  is referred to as the orientational order parameter.

Figure 3 shows the results of the density and order parameter profiles obtained for this confined system. The interface, or the region between the bulk and the wall, presents ordered layers that are densely packed and with an order parameter greater than zero. As one moves away from the walls, such influence vanishes and the bulk of the fluid is recovered. At this temperature the system's bulk is at the isotropic phase. The interface between the LC fluid and the wall, which posses orientational and positional order, will mainly shape the free energy landscape for a mesogen approaching a wall. Notice that the width of the inhomogeneity described by the two profiles is rather different: the density profile levels-off at  $z^* \approx 1.5$ , while the order parameter levels-off at  $z^* \approx 4.5$ . This is an adequate behaviour of the Gay-Berne model: in a real confined liquid crystal system, the orientational

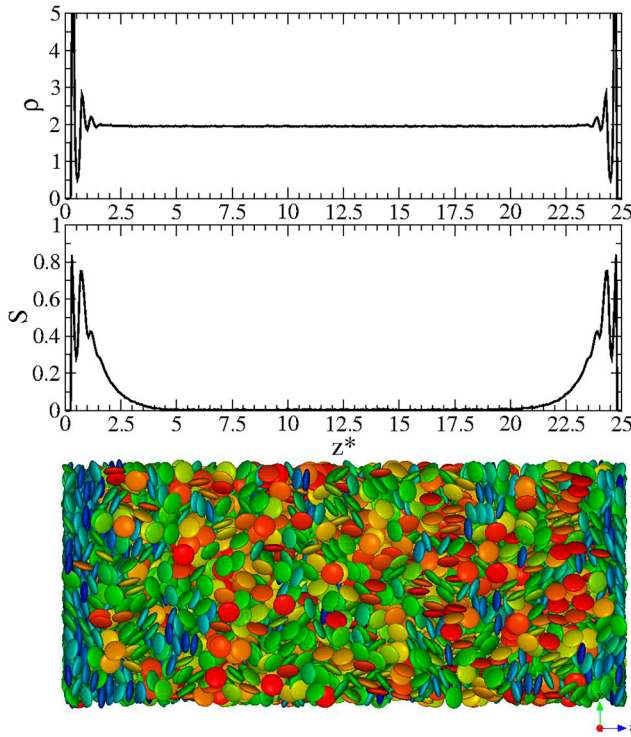


**Figure 3.** Snapshot of the DLC system studied at  $T^* = 3$ , and their corresponding density (upper) and order parameter (middle) profiles as a function of  $z^*$ .

order promoted via the anchoring of the walls extends farther than the positional order [33].

Further characterisation of the fluid interface can be obtained by the quasi-two-dimensional positional correlation function:

$$g(r_{xy}) = \frac{N(r_{xy})}{2\pi r_{xy} dr_{xy}}, \quad (5)$$

where  $r_{xy}$  stands for the  $xy$  projection of the distance between two particles,  $2\pi r_{xy} dr_{xy}$  stands for the area of a cell parallel to the wall of thickness  $dr_{xy}$ , and  $N(r_{xy})$  is the number of particles inside this cell. We have calculated  $g(r_{xy})$  within planar regions parallel to the wall and considering particles inside slabs of width of 0.4. Figure 4 includes the results for this pair correlation function calculated at four different distances from the walls:  $z^* = 0.35$  (black lines), 0.7 (red lines), 1.2 (green lines) and 1.5 (blue lines). Notice that the shape of the curve for the four layers is similar, although more pronounced peaks can be distinguished for layers that are closer to the wall. Only at the adjacent regions of the walls, the stratification of DLC presents a  $g(r_{xy})$  with a second and third peak.

At this point we will turn our attention to the process of calculating the potential of mean force. First we will describe the results obtained for the average force felt by a test particle and then we will discuss the results for the

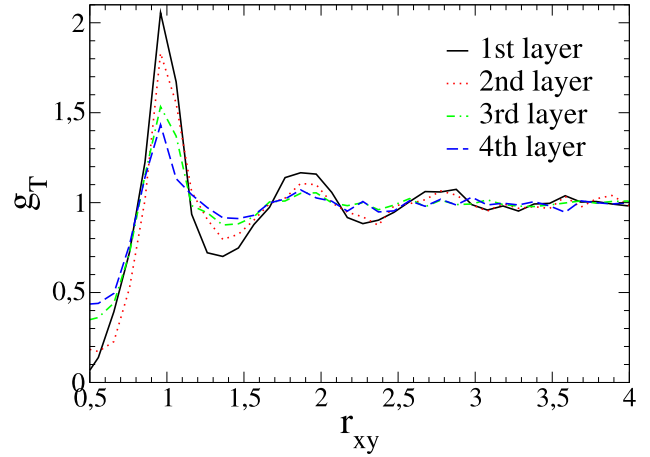


**Figure 4.** Quasi-two-dimensional pair correlation function ( $g_T = g(r_{xy})$ ) calculated at four different slabs near a wall:  $z^* = 0.35$  (black line), 0.7 (red line), 1.2 (green line) and 1.5 (blue line).

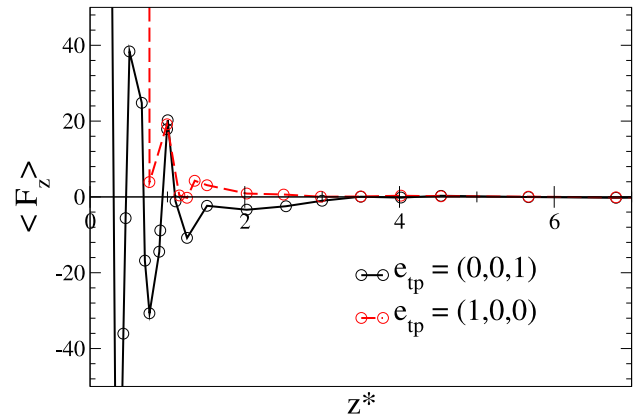


**Figure 5.** Average force in the  $z^*$  direction that the system exerts on the test particle as a function of the distance to the wall. The black line corresponds to the case where the test particle (tp) has an orientation vector  $\hat{e}_{tp} = (0, 0, 1)$ , while the red line stands for a test particle with  $\hat{e}_{tp} = (1, 0, 0)$ . The values reported correspond to an average over 25 different random  $x-y$  positions, and a time average over  $10^6$  simulation timesteps.

potential of mean force. Figure 5 shows the average forces in the  $z$ -direction that a test particle feels due to the rest of the fluid and the walls. The black line corresponds to the case where the test particle is aligned with the direction promoted by the anchoring, while the red line represents the case where the test particle lies perpendicular to the walls. In the first case, the unitary direction vector corresponds to  $\hat{e}_{tp} = (0, 0, 1)$ , while in the latter this vector corresponds to  $\hat{e}_{tp} = (1, 0, 0)$ . Notice that in the central part of the box the test particle, in both cases, feels no net force and only presents small fluctuations. This is to be expected: at the central part of the box the system's bulk presents an isotropic phase, where both, the position and orientation of the mesogens are completely random. In

such symmetric state all orientations are equivalent and the mesogens can explore freely positions and orientations without an effective opposition from the rest of the fluid.

When the test particle is closer to the more ordered slabs near the wall, the value of the average force is no longer zero. Let us discuss first the case where the test particle is ‘wrongly’ oriented. The red line in Figure 5, which corresponds to the case of the test particle with  $\hat{e}_{tp} = (1, 0, 0)$ , presents mainly positive values and globally decreases with  $z^*$ : at  $1.5 \leq z^* \leq 4$ , which corresponds to the inhomogeneous region depicted by the order parameter profile (Figure 3), the value of  $\langle F_z \rangle$  monotonically decreases until it levels off to zero at the bulk region. At  $0.5 \leq z^* \leq 1.5$ , the average forces presents oscillations due to the interaction with the layers formed near the wall, but with  $\langle F_z \rangle > 0$ . The fact that  $\langle F_z \rangle$  is positive, corresponds to a net push towards the centre of the cell.

In the case of the test particle aligned with the direction promoted by the anchoring of the wall, the scenario is different at the interface: for  $1.5 \leq z^* \leq 4$  the value of  $\langle F_z \rangle$  is negative and it increases until it levels off to the value of zero at the bulk. For  $0.24 \leq z^* \leq 1.5$  it oscillates due to the interaction with the layers formed near the wall, alternating between positive and negative values. In this case, the average force presents its negative values at positions which practically coincide with the centres of the ordered slabs near the wall ( $z^* \approx 0.345, 0.7, 1.2$ ). Hence, a negative force at this three regions reflects a net pull to the wall felt by the test particle. On the other hand, the positive value of  $F_z$  appears as soon as the test particle moves away from these layers and towards the wall. The positive sign is still the result of the attraction from an ordered column, but now pulling the test particle in the opposite direction. To summarise: in all cases there is an effective attraction felt by the test particle from these layers, but the sign of the average force changes depending on the position of the test particle.

Numerical integration of the mean force results in the potential of mean force. We have calculated such integral and averaged the PMF obtained for the 25 different samples. In Figure 6 we present these results: the black line corresponds to the PMF calculated for the test particles with the ‘right’ orientation ( $\hat{e}_{tp} = (0, 0, 1)$ ). The red line corresponds to the values of the PMF obtained for a test particle with the ‘wrong’ orientation ( $\hat{e}_{tp} = (1, 0, 0)$ ). The value of the PMF for a given position  $z_i^*$ , represents the change of the Helmholtz energy between two states: the initial state where a particle with a fixed orientation is located at  $z^* = 11$ , and the final state where the same particle keeps its orientation at position  $z_i^*$ .

The PMF shows no dependence in the  $x$ – $y$  coordinates but only on the distance to the wall. This is to be

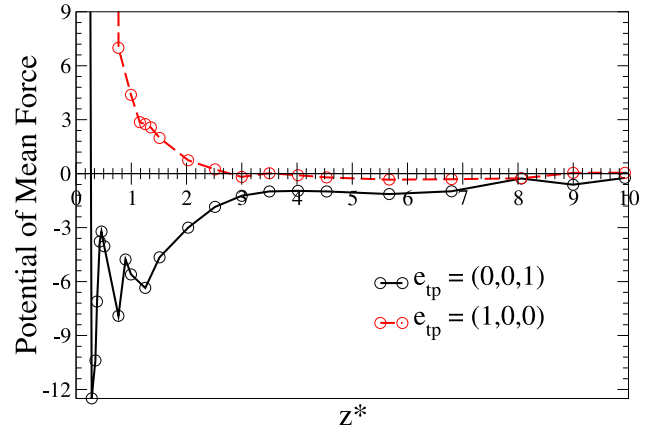


**Figure 6.** Potential of mean force. The black line corresponds to the case where the test particle (tp) has an orientation vector  $\hat{e}_{tp} = (0, 0, 1)$ , while the red line stands for a test particle with  $\hat{e}_{tp} = (1, 0, 0)$ . The values reported correspond to an average over 25 different random  $x$ – $y$  positions, and a time average over  $10^6$  simulation timesteps.

expected: as it is depicted in Figure 4, inside the layers formed at the interface (which are parallel to the wall) the radial distribution function  $g(r_{xy})$  behaves as a fluid, this is, there is no intra-layer positional order at the interface.

Notice that the inclusion of a test particle produces a perturbation on the density and order parameter of the fluid particles around it, especially for a test particle with the ‘wrong’ orientation. This has an important contribution in the calculation of the PMF which is primarily due to the fluid particles near the test one. On the other hand, an increase in the  $x$ – $y$  cross sectional area will only add a small contribution on the PMF arising from fluid particles that are far from the test particle and where the perturbation has been washed out. Nonetheless, a sufficiently large simulation box (with a large  $x$ – $y$  cross sectional area) is needed to minimise finite-size effects, as usual in simulations using periodic boundary conditions. To obtain a practical minimum size where these finite-size effects are important is not straightforward since it will depend on the parameters of the system like cell thickness, density, and others. We have chosen the number of simulation particles  $N = 5000$  (and thus of the  $x$ – $y$  cross sectional area for the given cell thickness) to ensure that finite-size effects are negligible.

With regard to the behaviour of the PMF across the entire cell, we will again discuss first the results for the ‘wrongly’ oriented test-particle (red line in Figure 6). Although there are small fluctuations observed, overall, the PMF behaves as a decreasing function of  $z^*$ .

The PMF obtained with the test particle ‘rightly’ oriented overall behaves as an increasing function of  $z^*$ . At the interface, the PMF presents three different minima

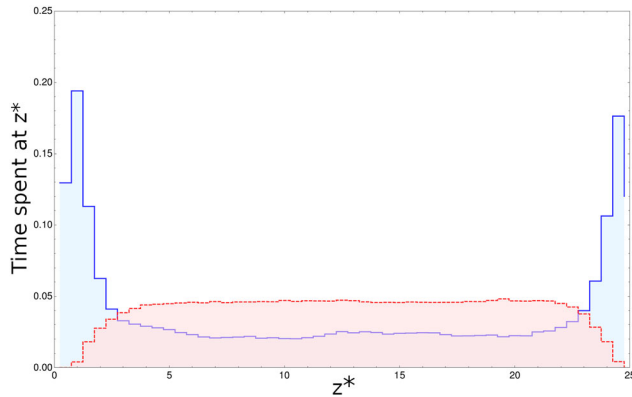


**Figure 7.** Histogram with the relative time spent on a given  $z^*$  position for two particles with fixed orientations: blue line corresponds to a particle with  $\hat{e}_{tp} = (0, 0, 1)$ , while the red line corresponds to a particle with  $\hat{e}_{tp} = (1, 0, 0)$ . The histograms have a normalised area of 1.

around  $z^* \approx 0.345, 0.7, 1.2$ . The global minimum of the function is around  $z^* \approx 0.345$ , while the two other values correspond to local minima; the depth of the three minima increases as they are closer to the wall. This means that a particle which is aligned with the anchoring promoted by the wall, will be effectively attracted to the wall, promoting the adsorption of particles with this orientation.

In order to gain further insight on the role that a particle's orientation has on its dynamics, we have calculated an histogram with the relative time that a particle, with a fixed orientation, spends in a given  $z$ -region of the cell. The histogram shown in Figure 7 was obtained by performing  $NVT$  simulations for  $1 \times 10^7$  timesteps of 5000 particles, and by normalising the value of its area. For this simulations, among the discs, a particle is included which interacts with the rest of the fluid and is able to translate according to the dynamical equations but is not able to rotate. The blue line in Figure 7 summarises the result for

a particle with  $\hat{e}_{tp} = (0, 0, 1)$ , and the red line stands for a particle with  $\hat{e}_{tp} = (1, 0, 0)$ .

According to the histogram, a particle whose direction is  $\hat{e}_{tp} = (0, 0, 1)$  (blue rectangles), will visit often the region where the PMF presents its global minimum and will spend most of its time at the interface. On the other hand, the histogram obtained for the particle with  $\hat{e}_{tp} = (1, 0, 0)$ , shows that the interface is practically a forbidden region for a disc with this orientation. This is in agreement with the results obtained with the PMF.

Up to now we have only considered two main orientations of the mesogens. A natural question arises about the behaviour of particles with intermediate orientations. Hence, we calculated the PMF for test particles whose orientation is intermediate between  $\hat{e}_{tp} = (1, 0, 0)$  and  $(0, 0, 1)$ . We have specifically considered the orientation vectors:  $(\frac{\sqrt{3}}{2}, 0, \frac{1}{2})$ ,  $(\frac{1}{\sqrt{2}}, 0, \frac{1}{\sqrt{2}})$  and  $(\frac{1}{2}, 0, \frac{\sqrt{3}}{2})$ , which correspond to rotations of 30, 45 and 60 degrees going from  $(1, 0, 0)$  to  $(0, 0, 1)$ . Figure 8 includes the results of the average force obtained with these test particles and their corresponding PMF. The orange line stands for the PMF where the test particle has been rotated by 30 degrees from  $(1, 0, 0)$ , the cyan line represents a particle rotated by 45 degrees, and, finally, the blue line stands for the 60 degrees rotation.

The average force obtained for  $\hat{e}_{tp} = (\frac{\sqrt{3}}{2}, 0, \frac{1}{2})$  is depicted in orange in Figure 8(a). Note the similitude with the dashed red line which stands for the  $\hat{e}_{tp} = (1, 0, 0)$  case, at least in the region where  $z^* \geq 0.75$ . At distances closer to the wall, the force presents a global minimum at  $z^* \approx 0.5$ , and then grows due to the repulsive interaction with the wall. This is interesting, since a disc which is slightly rotated from the orientation  $(1, 0, 0)$  could find at least one region inside the interface where it is effectively attracted to the corresponding wall. This information is more clearly presented by the PMF. The

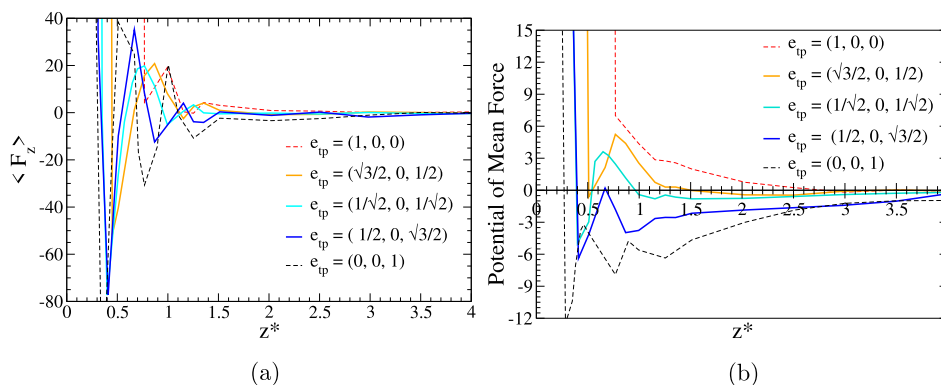


**Figure 8.** (a)  $\langle F_z \rangle$  profile obtained for five different orientations: dashed red line corresponds to a particle with an edge-on orientation, while the dashed black line corresponds to the face-on orientation. The orange, cyan and blue lines correspond to intermediate orientations between the latter two cases, specifically: 30, 45 and 60 degrees going from the edge-on orientation into the face-on, respectively. (b) Potential of mean force obtained for the same five cases depicted in (a) and with the same colour code.

orange line in Figure 8(b) shows that for  $z^* \geq 0.75$  this PMF is a decreasing function of  $z^*$ . The other curves show similar behaviour.

## 5. Conclusions

In this study we have quantified the orientational dependence of the energy landscape for a system of DLC particles, confined between two walls promoting a face-on anchoring. We have specifically studied two limiting cases where  $\hat{e}_{tp} = (0, 0, 1)$  and  $\hat{e}_{tp} = (1, 0, 0)$ , in other words, orientations of the test particle which are parallel and perpendicular to the anchoring of the wall, respectively. Also, three intermediate cases were explored where the test particle has  $\hat{e}_{tp} = (\frac{\sqrt{3}}{2}, 0, \frac{1}{2})$ ,  $(\frac{1}{\sqrt{2}}, 0, \frac{1}{\sqrt{2}})$  and  $(\frac{1}{2}, 0, \frac{\sqrt{3}}{2})$ .

Interestingly, our results show that the PMF extends further than the wall-disc potential due to the preferred orientation of the fluid promoted by the wall. In the face-on case ( $\hat{e}_{tp} = (0, 0, 1)$ ) the PMF depicts an effective attractive interaction, with three different local minima due to the layers of the inhomogeneous region near the wall. These positions of local minima coincide with the positions where the density presents their local maxima, meaning that a particle inside the structured fluid will be attracted by these fluid layers. Nevertheless, the global minimum of the PMF is located adjacent to the wall and, hence, any mesogen oriented according to the orientation imposed by the anchoring of the wall, will feel an effective attraction towards the wall.

As the orientation of the test particle diverts from the face-on case and approaches to an edge-on orientation, the minima of the PMF move farther from the wall and become shallower. Finally, in the edge-on case ( $\hat{e}_{tp} = (1, 0, 0)$ ) the PMF is purely repulsive and decreases monotonically as a function of the distance to the wall. This happens in contrast to the behaviour of the wall-disc potential which, independently of the particle's orientation, always contains an attractive term (see Figure 1).

Calculations such as those carried out in this work could be useful, for example, to obtain anisotropic effective surface potentials, that in turn could be used in density functional theory.

Even though there are other simulation techniques for calculating the PMF with high resolution [14, 34, 35], the method used in this study is convenient given that the calculation of the forces over all the fluid particles is an intrinsic part of the MD algorithm.

## Acknowledgments

The IPICYT's National Supercomputing Center supported this research with the computational time grant TKII-R2018-DSB1.

CIM acknowledges partial financial support from DGAPA-UNAM grant number IN-103419. The authors would also like to thank the supercomputing resources provided by DGTIC-UNAM and UAM at Mexico City, Mexico.

## Disclosure statement

No potential conflict of interest was reported by the author(s).

## Funding

The IPICYT's National Supercomputing Center supported this research with the computational time grant TKII-R2018-DSB1. CIM acknowledges partial financial support from DGAPA-UNAM grant number IN-103419.

## ORCID

Daniel Salgado-Blanco  <http://orcid.org/0000-0002-2527-3027>

## References

- [1] G.H. Heilmeyer and L.A. Zanoni, *Appl. Phys. Lett.* **13**, 91 (1968).
- [2] V. Shibaev, A. Bobrovsky, and N. Boiko, *Progr. Polym. Sci.* **28**, 729–836 (2003).
- [3] I.C. Khoo, *Phys. Rep.* **471**, 221–267 (2009).
- [4] M. Kumar and S. Kumar, *Polym. J.* **49**, 85–111 (2017).
- [5] A. Sengupta, *Int. J. Mol. Sci.* **14**, 22826–22844 (2013).
- [6] A. Sengupta, S. Herminghaus, and C. Bahr, *Liq. Crys. Rev.* **2**, 73–110 (2014).
- [7] R. Zhang, T. Roberts, I.S. Aranson, and J.J. de Pablo, *J. Chem. Phys.* **144**, 084905 (2016).
- [8] T.T. Alkeskjold, L. Scolari, D. Noordegraaf, J. Lægsgaard, J. Weirich, L. Wei, G. Tartarini, P. Bassi, S. Gauza, S.-T. Wu, and A. Bjarklev, *Opt. Quant. Electron.* **39**, 1009–1019 (2007).
- [9] H.K. Bisoyi and S. Kumar, *Chem. Soc. Rev.* **39**, 264–285 (2010).
- [10] N. Kasch, *Liq. Cryst. Today* **21**, 76–77 (2012).
- [11] T. Seki, S. Nagano, and M. Hara, *Polymer* **54**, 6053–6072 (2013).
- [12] J. Hoogboom, J.A.A.W. Elemans, T. Rasing, A.E. Rowan, and R.J.M. Nolte, *Pol. Int.* **56**, 1186–1191 (2007).
- [13] Y. Yi, M. Nakata, A.R. Martin, and N.A. Clark, *Appl. Phys. Lett.* **90**, 163510 (2007).
- [14] E.B. Kim, R. Faller, Q. Yan, N.L. Abbott, and J.J. de Pablo, *J. Chem. Phys.* **109**, 7737–7744 (2002).
- [15] W. Billes, F. Bazant-Hegemark, M. Mecke, M. Wendland, and J. Fischer, *Langmuir* **19**, 10862–10868 (2003).
- [16] E.B. Kim, O. Guzmán, S. Grollau, N.L. Abbott, and J.J. de Pablo, *J. Chem. Phys.* **121**, 1949–1961 (2004).
- [17] E.B. Kim and J.J. de Pablo, *Phys. Rev. E* **69**, 061703 (2004).
- [18] M. Müller and J.J. de Pablo, *Lect. Notes Phys.* **703**, 67–122 (2006).
- [19] C.D. Christ, A.E. Mark, and W.F. van Gunsteren, *J. Comput. Chem.* **31**, 1569–1582 (2010).
- [20] A. Pohorille, C. Jarzynski, and C. Chipot, *J. Phys. Chem. B* **114**, 10235–10253 (2010).
- [21] D.J. Cleaver, C.M. Care, M.P. Allen, and M.P. Neal, *Phys. Rev. E* **54**, 559–567 (1996).

- [22] L. Bellier-Castella, D. Caprion, and J.-P. Ryckaert, *J. Chem. Phys.* **121**, 4874–4883 (2004).
- [23] D. Salgado-Blanco, E. Díaz-Herrera, and C.I. Mendoza, *J. Phys. Condens. Matter* **31**, 105101 (2019).
- [24] M.A. Bates and G.R. Luckhurst, *J. Chem. Phys.* **110**, 7087–7108 (1999).
- [25] M. Sprik and G. Ciccotti, *J. Chem. Phys.* **109**, 7737–7744 (1998).
- [26] J.M. Ilnytskyi and M.R. Wilson, *Comput. Phys. Commun.* **148**, 43–58 (2002).
- [27] S.K. Pal, S. Setia, B.S. Avinash, and S. Kuma, *Liq. Cryst.* **40**, 1769–1816 (2013).
- [28] M. Rahimi, T.F. Roberts, J.C. Armas-Pérez, X. Wang, E. Bukusoglu, N.L. Abbott, and J.J. de Pablo, *PNAS* **112**, 5297–5302 (2015).
- [29] O. Lavrentovich, B. Lev, and A. Trokhymchuk, *Condens. Matter Phys.* **13**, 30101 (2010).
- [30] G. Carbone, G. Lombardo, R. Barberi, I. Musevic, and U. Tkalec, *Phys. Rev. Lett.* **103**, 167801 (2009).
- [31] R. Zhang, X. Zeng, B. Kim, R.J. Bushby, K. Shin, P.J. Baker, V. Percec, P. Leowanawat, and G. Ungar, *ACS Nano* **9**, 1759–1766 (2015).
- [32] R. Eppenga and D. Frenkel, *Mol. Phys.* **52**, 1303–1334 (1984).
- [33] B. Jérôme, *Rep. Progr. Phys.* **54**, 391–451 (1991).
- [34] J. Kästner, *WIREs Comput. Mol. Sci.* **1**, 932–942 (1991).
- [35] L. Zheng, M. Chen, and W. Yang, *PNAS* **105**, 20227–20232 (2008).